Arabian Journal of Chemistry (2020) 13, 8898–8908

King Saud University

Arabian Journal of Chemistry

www.ksu.edu.sa
www.sciencedirect.com

ORIGINAL ARTICLE

# Schiff base stabilized silver nanoparticles as potential sensor for Hg(II) detection, and anticancer and antibacterial agent

**Aaliya Minhaz [a,b,c,*], Naeem Khan [d], Nargis Jamila [a,**], Fatima Javed [a], Muhammad Imran [c], Shaukat Shujah [d], Sadiq Noor Khan [e], Amir Atlas [d], Muhammad Raza Shah [b]**

[a] *Department of Chemistry, Shaheed Benazir Bhutto Women University, Peshawar 25000, Khyber Pakhtunkhwa, Pakistan*
[b] *International Centre for Chemical and Biological Sciences, HEJ Research Institute of Chemistry, University of Karachi, Sindh, Pakistan*
[c] *Institute of Chemical Sciences, University of Peshawar, Peshawar 25120, Khyber Pakhtunkhwa, Pakistan*
[d] *Department of Chemistry, Kohat University of Science and Technology, Kohat 26000, Khyber Pakhtunkhwa, Pakistan*
[e] *Department of Medical Laboratory Technology, University of Haripur, Haripur 22060, Khyber Pakhtunkhwa, Pakistan*

Received 22 August 2020; accepted 8 October 2020
Available online 22 October 2020

**KEYWORDS**

Silver nanoparticles;
Hg(II) sensor;
Tap water;
Redox;
Anticancer

**Abstract** This study reports a facile synthesis of silver nanoparticles (C3-AgNPs) by chemical route, using C3; 2,2′-((1E,1′E)-(propane-1,3-diylbis(azanylylidene))bis(methanylylidene))diphenol (**3**) and silver nitrate. The formation of nanoparticles was monitored using UV–Vis spectroscopy by the appearance of typical surface plasmon absorption maxima. The synthesized C3-AgNPs were characterized using Fourier-Transform-infrared (FTIR) and atomic force microscopy (AFM) techniques. In addition, the effect of concentration, temperature, time, pH, and stability in salts solution on C3-AgNPs was determined. From AFM, C3-AgNPs were found polydispersed with average size of 29.93 nm. Furthermore, the study reports C3-AgNPs as sensitive protocol for the detection of toxic metal; Hg(II) in tap water. From ten salts tested, C3-AgNPs demonstrated a sensitive and selective spectrophotometric signal and aggregation induced decrease of surface plasmon resonance (SPR) band. The nanosensor probe displayed a sensitive response to Hg(II) in a wide range of concentrations and pH. In addition, the decrease in SPR band of C3-AgNPs due to Hg(II) was not affected by tap water samples. C3-AgNPs also exhibited a redox catalytic potential in dyes degradation. In biological application, C3-AgNPs exhibited significant anticancer and antibacterial potential of 65 to 94% at

* Corresponding author at: Department of Chemistry, Shaheed Benazir Bhutto Women University, Peshawar, Khyber Pakhtunkhwa, Pakistan.
** Corresponding author at: Department of Chemistry, Shaheed Benazir Bhutto Women University, Peshawar, Khyber Pakhtunkhwa, Pakistan.
E-mail addresses: aaliyachem@sbbwu.edu.pk (A. Minhaz), nargisjamila@sbbwu.edu.pk (N. Jamila).
Peer review under responsibility of King Saud University.

Production and hosting by Elsevier

https://doi.org/10.1016/j.arabjc.2020.10.016

24–72 h, and inhibition zone of 7–18 mm, respectively. Hence, the synthesized C3-AgNPs could have promising application in environmental and pharmacological remediation.



## 1. Introduction

The recognition and sensing of heavy and transition metal ions has emerged as a significant goal in the field of chemical sensors in recent years (Ding, 2019; Patil and Das, 2019; Rao et al., 2019; Modrzejewska-Sikorska and Konował, 2020). Metal nanoparticles (MNPs) have significant applications as colorimetric sensors in the detection of biomolecules, metallic ions, and several diseases (Tan et al., 2012; Bothra et al., 2013; Guo et al., 2017; Zhang et al., 2017; Elahi et al., 2018; Sun et al., 2019). Due to unique optical properties, AgNPs have strong surface plasmon resonance (SPR) absorption properties depending on size, shape, and inter-particle distances (Burda et al., 2005). MNPs based electrodes have been previously used to detect toxic ions (Zhao et al., 2017; Pungjunun et al., 2018). In this modern era, mankind is exposed to the highest levels of toxic metals due to industrialization, fuels, and incineration of waste materials worldwide. Among them, mercury (Hg) is a hazardous pollutant and bioaccumulative neurotoxin emitted into the atmosphere through natural as well as anthropogenic activities, in gaseous elemental (major), gaseous oxidized, or particulate bound mercury form. The oxidized and particulate bound forms due to their high solubility are removed fast from the atmosphere via wet and dry deposition; the primary pathways for Hg to enter terrestrial and aquatic ecosystems (Ye et al., 2019). This Hg deposition causes lethal health damages to the living organisms. Therefore, to ensure the environment safety, it is crucial to design the robust and efficient methods to monitor, quantify, and remove Hg traces from the environment including water, soil, and plants.

In the past, traditional methods used for Hg quantification include atomic absorption spectroscopy, inductively coupled plasma (ICP) -optical emission spectroscopy (OES), ICP-mass spectrometry, and direct mercury analyzer (DMA) (Hwang et al., 2016; Hong et al., 2019; Švehla et al., 2019). These all methods exhibit high sensitivity and efficiency, but involve long analysis time, complicated operations and high cost. Therefore, a development of simple, cost-effective, rapid, sensitive, and validated method is required for the real time Hg detection.

Recently, the use of MNPs as colorimetric sensors for waterborne contaminants/pollutants have attracted considerable attention due to cost effectiveness, and protocols and operational simplicity (Anwar et al., 2018). It has been recently seen that in sensing of several heavy metal cations, some Schiff bases derivatives demonstrated excellent sensitivity and selectivity due to their distinguished coordinative proficiency (Dong et al., 2019; Jia et al., 2019; Salarvand et al., 2019). MNPs, particularly silver nanoparticles (AgNPs) with well-dispersed size due to their unique optical SPR peak, lies in the visible region. In addition, the role of MNPs as colorimetric sensors for metallic ions detection is mainly concomitant with their surface modification using stabilizing agents such as ligand or bio-molecules, which interact through metal–ligand co-ordination (Auría-Soro et al., 2019; Samerjai et al., 2019; Balachandramohan and Sivasankar, 2020). In continuation to our previous investigation (Anwar et al., 2016), in this research work, a highly selective and sensitive method using AgNPs modified with a new Schiff base; 2–2′–((1E, 1E')–(propane–1,3 diylbis(azanylidene))bis(methany–lidene))diphenol, C3 (Scheme 1) was developed for the detection and quantification of Hg(II) in real water sample of Peshawar.

Nowadays, organic dyes, which are used as colorant in textile, paper, food, drug, cosmetics, leather and printing industries are seriously contaminating water, and are highly toxic to terrestrial as well as aquatic systems. As the recent methods for toxic contaminants removal such as use of sodium borohydride ($NaBH_4$) are expensive, kinetically unfavourable, and inefficient, therefore, to design ecofriendly and low cost techniques for dyes degradation into functional products is of great concern. Recently, the catalytic reduction/degradation of dyes by biogenic NPs has received the great attention of researchers (Ali et al., 2017; Singh et al., 2018; Khan et al., 2019). Hence, the current study also investigates the catalytic application of the synthesized C3-AgNPs in organic dyes including methylene blue (MB) and Congo red (CR) reduction and degradation.

Silver nanoparticles due to enhanced permeability, biocompatibility, and retention effect, play a key role in the treatment of diseases, drug delivery, and medicine, specifically in detecting, targeting, and treating tumor sites/cancer cells. Additionally, AgNPs due to excessive reactive oxygen species (ROS) production and DNA damage have also been reported to exhibit significant antibacterial activities (Bello et al., 2017; Kumari et al., 2020). Keeping this importance of AgNPs into consideration, in this study, the synthesized C3-AgNPs were examined for anticancer activity against prostate cancer cell line (DU-145), and antibacterial capabilities against *Staphylococcus aureus*, *Bacillus subtilis, Pseudomonas aeruginosa*, and *E. coli*. This is the first report on the synthesis of AgNPs using the subject synthesized new Schiff base (C3), and evaluating the sensing property, anticancer, and antibacterial potential of the modified AgNPs.

## 2. Materials and methods

### 2.1. Chemicals

$AgNO_3$ (99%), sodium borohydride ($NaBH_4$; 99%), prostate cancer cell line (DU-145), normal fibroblasts (L-929), and dyes (CR, MB) were purchased from Merck and Sigma Aldrich. Compound, C3 was synthesized in the laboratory following Scheme 1. Microbial strains; *Staphylococcus aureus, Bacillus subtilis, Pseudomonas aeruginosa, Escherichia coli* of ATCC 29213, 19659, 17588, and 25922, respectively, Muller Hinton agar and Broth (MHA and MHB) *p*-iodonitrotetrazolium chloride, and vancomycin and streptomycin (standards) were

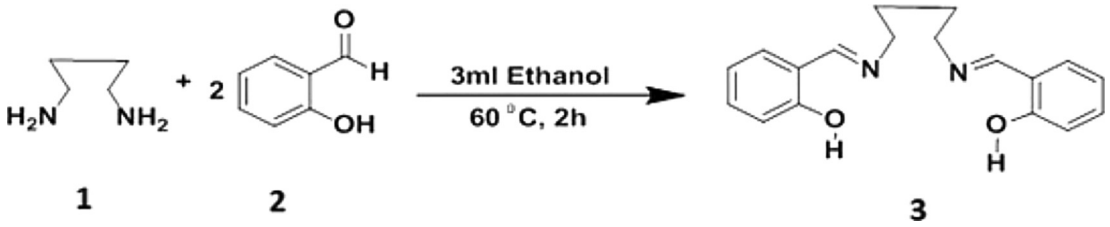


**Scheme 1** Schematic representation for the synthesis of Schiff base, C3 (**3**).

procured from Oxoid (England), Sigma-Aldrich (USA) and Duchefa Biochemie (Netherlands).

### 2.2. Instrumentation

A UV–Vis spectrophotometer (Shimadzu, UV-1800 spectrophotometer) in a range of 200–700 nm, Shimadzu FT-IR (model IR prestige 21 spectrophotometer) in a range of 400–4000 $cm^{-1}$, and a Bruker AV-600 MHz NMR spectrometer (Fallenden, Switzerland) were used for confirming C3-AgNPs synthesis, functional groups involved in the subject AgNPs production, and confirmation of C3 (ligand) synthesis, respectively. AFM images were recorded using 5500 AFM (Agilent Technologies, USA) at a scan rate of 0.5 Hz. AFM analysis of surface topography was carried out in ambient conditions using a multimode AFM with Nanoscope IIIa controller (Bruker Corporation, Billerica, MA, USA) and a vertical engagement (JV) 125 μm scanner. Contact mode was silicon–nitride tips (NP-20, Bruker, nominal frequency 56 kHz, nominal spring constant of 0.32 N/m) and a scan resolution of 512 samples per line was used throughout the analysis (Jamila et al., 2020). The images were plotted by NanoScope™ software (version V614r1; Digital Instruments, Tonawanda, NY, USA).

### 2.3. Synthesis of Schiff base (C3)

Ligands such as Schiff bases are considered as one of the most famous families of organic compounds, which are used as synthetic intermediates in coordination chemistry and stabilization of MNPs. C3 was synthesized according to Scheme (1). Briefly, a solution of 1.0 mM putrescine (**1**) and 2.0 mM salicylaldehyde (**2**) were mixed in 3 mL HPLC grade ethanol, and the reaction mixture was stirred at 60 °C for 2 h (Scheme 1). The reaction completion was monitored by TLC in a solvent system of dichloromethane:methanol (9:1). After reaction completion, the solvent was evaporated under reduced pressure, and a solid residue of crude product C3 (**3**) was obtained and recrystallized from 1:1 mixture of dichloromethane and methanol to yield C3; 2-2′-((1E,1E′)-(p-ropane-1,3-diylbis(azanylidene))bis(methanylidene))diphenol. The UV–Vis and $^1$H NMR spectra of C3 ligand are given in Fig. 1.

### 2.4. Synthesis of C3 stabilized silver nanoparticles (C3-AgNPs)

For the synthesis of C3-AgNPs, 0.1 mM ligand in 10% methanol and deionized water, and 0.1 mM $AgNO_3$ in deionized water were stirred for 30 min. Then, 0.1 mL of freshly prepared $NaBH_4$ solution (4.0 mM, in deionized water) was added drop by drop to the reaction mixture (Anwar et al., 2016). Formation of C3-AgNPs was indicated by color changes of reaction mixture (light yellow to dark brown). After constant stirring for 3 h, the reaction mixture was subjected to UV–Vis analysis. To determine the optimum synthesis of C3-AgNPs, different ratios of C3 and $AgNO_3$ (1:1, 1:2, 1:5, 1:15, 1:20, 2:1, 5:1) were employed. The synthesized C3-AgNPs were collected by centrifugation and washing thoroughly with deionized water. The final product of C3-AgNPs was vacuum dried at 105 °C for 3 h. Furthermore, the effect of several parameters such as concentration, temperature, time, pH, and stability in salts solution on C3-AgNPs was determined.

### 2.5. Detection of Hg(II) ions and analytical performance via C3-AgNPs

For analyzing chemosensing property of the subject synthesized C3-AgNPs, 10 different metal salt solutions; Ag(I), Co (I), Cu(I), Na(I), K(I), Rb(I), Ba(II), Cd(II), Fe(II), Sb(II), Sb(III), Fe(III) of 0.1 mM were mixed in 1:1 (v/v) ratio with 0.1 mM C3-AgNPs. To demonstrate the sensitivity of C3-AgNPs based Hg(II) sensing, several Hg(II) concentrations (0.01 μM to 50 μM) were titrated against C3-AgNPs. The limits of detection and quantification (LOQ, LOQ) for Hg(II) ions were calculated as three and ten times standard deviations (3xSD and 10xSD) from ten replicates of blank per slope of the calibration curve.

### 2.6. C3-AgNPs as catalysts in MB and CR degradation

The catalytic activity of C3-AgNPs against CR and MB was analyzed according to the published literature (Jamila et al., 2020). The degradation of dyes was indicated by the decolorization of solution and analysis via UV–visible spectrophotometer.

### 2.7. Anticancer and antibacterial activities of C3-AgNPs

Anticancer potential of the synthesized C3-AgNPs was analyzed via lactate dehydrogenase (LDH) assay according to published method (Jamila et al., 2014). To determine the cytotoxicity of C3-AgNPs (100 μg/mL in DMSO) on prostate cancer and normal cells (DU-145 and L-929), a cytotoxicity kit was used, which determines the released amount of LDH. Antibacterial activity was evaluated using slightly modified disc diffusion and broth micro-dilution methods. The bacterial strains were *Bacillus subtilis*, *Staphylococcus aureus*, *Pseudomonas aeruginosa*, and *Escherichia coli*. In disc diffusion assay, a 100 μL inoculum was patterned on the MHA surface. Then, filter paper disc steeped with C3 and C3-AgNPs (20 μL of 2000 μg/mL), and the standard drugs (streptomycin, vancomycin) were kept on the inoculated agar. The petri dishes

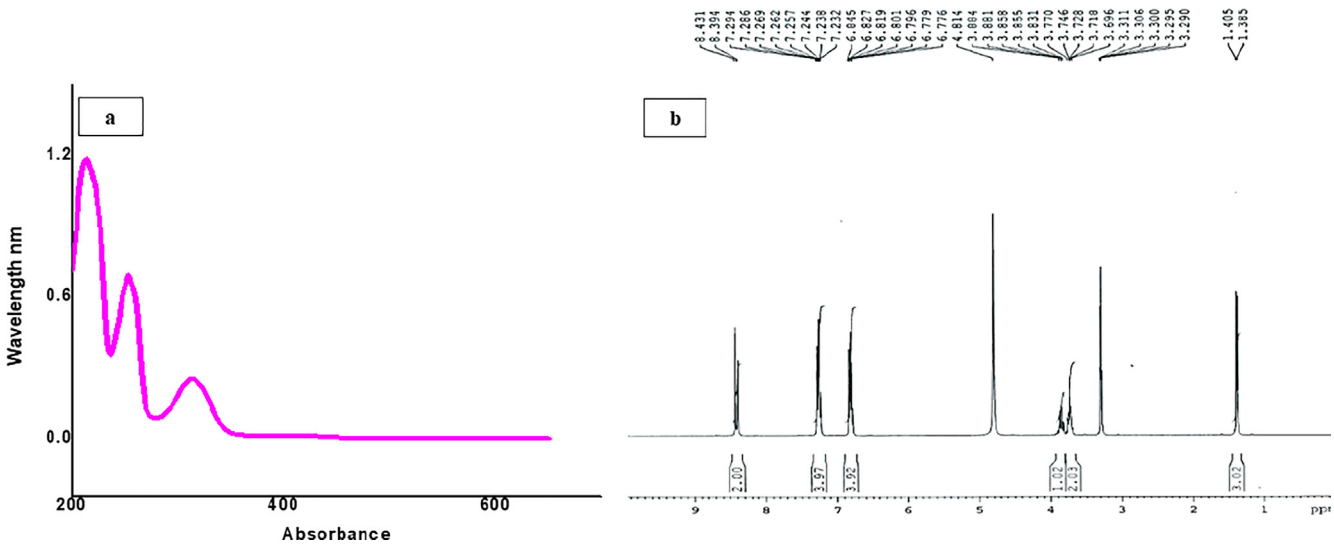


**Fig. 1** (a) UV–Vis and (b) $^{1}H$ NMR spectra of C3 Schiff base (**3**).

were then incubated at 37 °C overnight. The diameter of inhibition zones were recorded in millimeters (mm). Furthermore, broth micro-dilution assay (minimal inhibitory concentration, MIC) with 1000–31.25 μg/mL concentration was performed using 96-well plate.

### *2.8. Statistical analysis*

The results of antibacterial activity in disc diffusion and MIC are reported as means ± standard deviations of three replicates. The significant differences in the mean values are represented by superscript letters, which were obtained by ANOVA and Tukey's HSD test in SPSS, version 20.0 at a significance level of $p < 0.05$.

## 3. Results and discussion

### *3.1. Synthesis and spectral properties of C3-AgNPs*

In this research work, a one phase strategy of C3-AgNPs synthesis was designed using simple and rapid reduction of $AgNO_3$ by $NaBH_4$ in the presence of stabilizing agent, C3 Schiff base (1:9, acetonitrile:deionized water). Various ratios of C3 and $AgNO_3$ were mixed to optimize the stability of C3-AgNPs (Fig. 2). Comparing different ratios (1:1, 1:2, 1:5, 1:15, 1:20, 2:1, 5:1), the ratio 1:15 (v/v, C3:$AgNO_3$) demonstrated the highest absorbance as indicated by the well stable, and prominent SPR peak exhibited at 390 nm region in a time of 15 min (Fig. 2) indicating $Ag^{+}$ reduction to $Ag^{0}$ and polydispersed AgNPs formation. The results further indicated that by increasing a ratio of $AgNO_3$ solution (Fig. 2), the size of C3-AgNPs gradually decreases.

### *3.2. Detection of Hg(II) ions via C3-AgNPs*

In the analysis to detect Hg(II) ions via C3-AgNPs, the obtained results showed that the addition of Hg(II) to C3-AgNPs caused decolorization as well as the disappearance

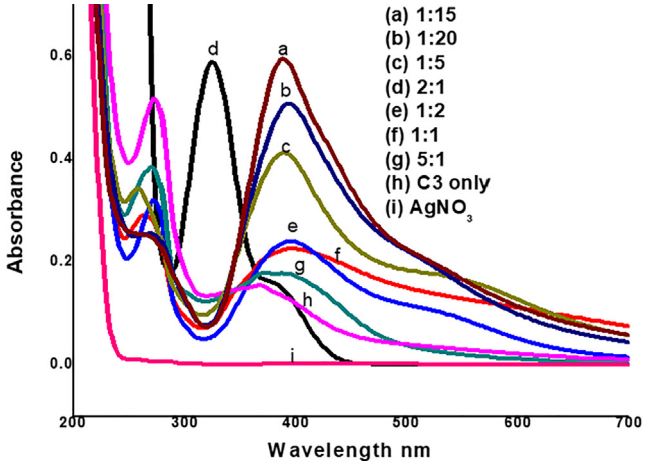


**Fig. 2** UV–Vis spectra of different ratios of C3 and $AgNO_3$ solution for optimizing synthesis of C3-AgNPs.

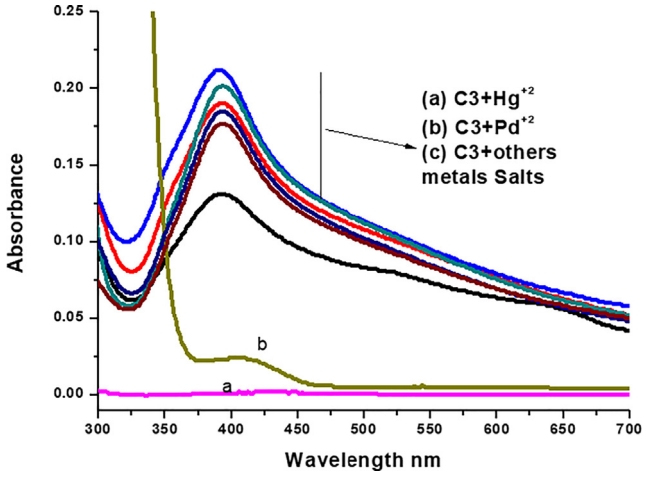


**Fig. 3** UV–Vis spectra showing the effect of various salt solutions after addition to C3-AgNPs.

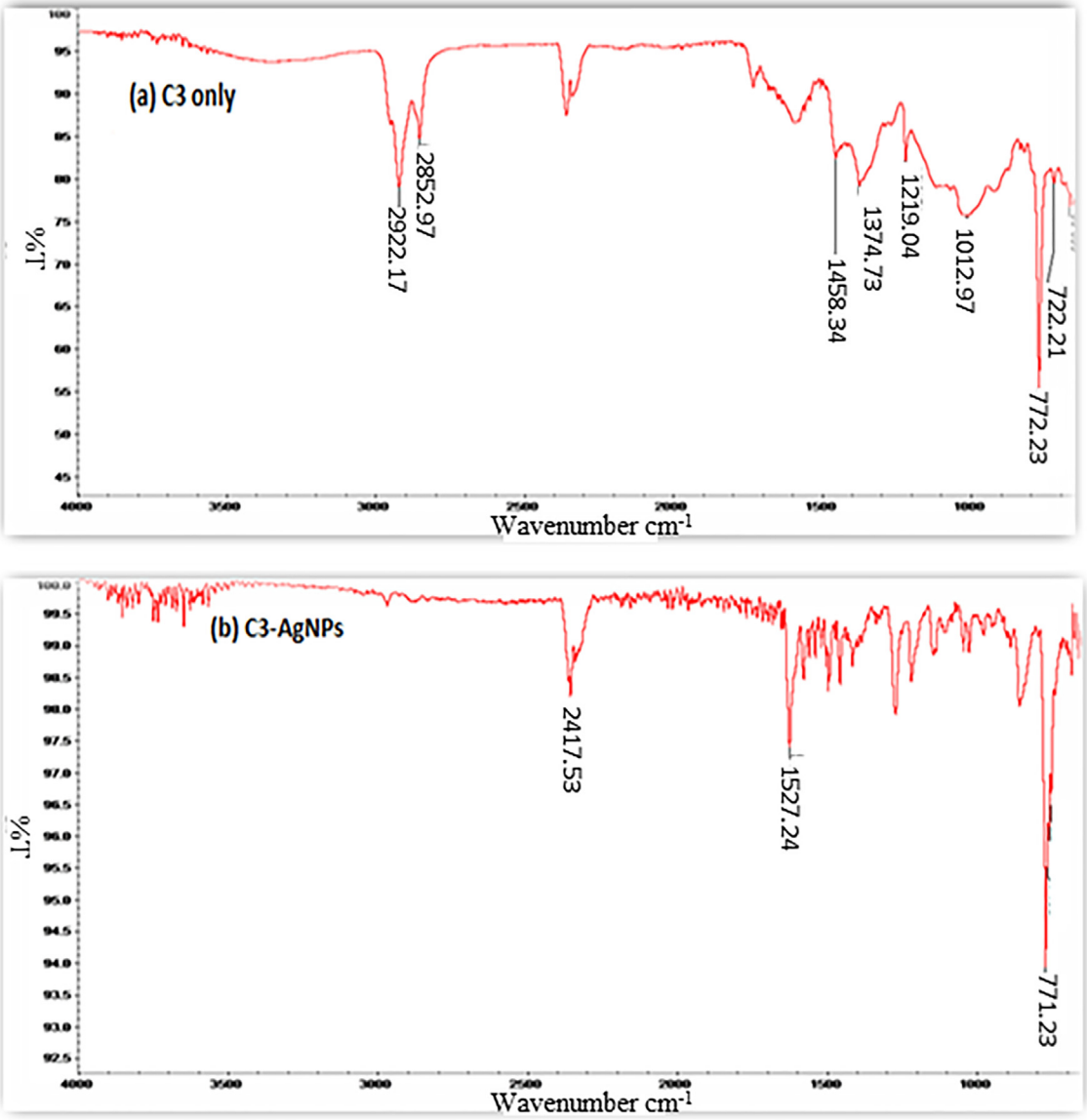


**Fig. 4** FTIR spectra of (a) C3, **3** (b) C3-AgNPs.

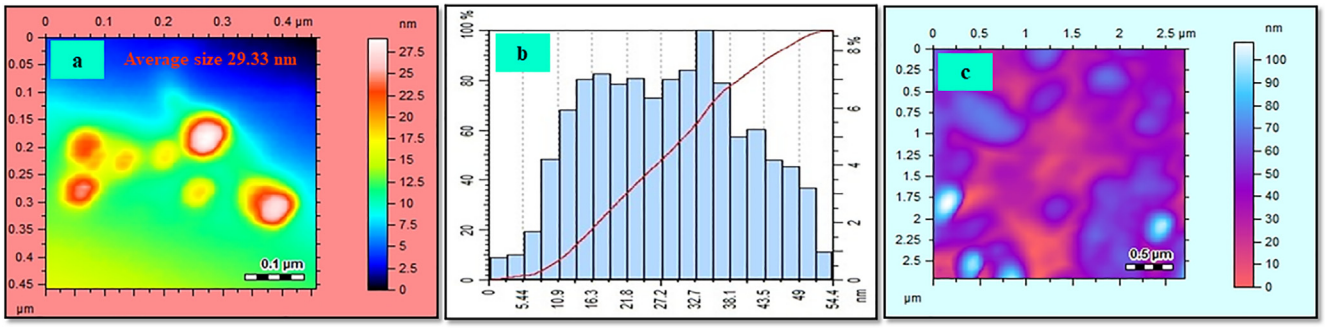


**Fig. 5** (a) AFM image, (b) size distribution curve of C3-AgNPs, and (c) AFM image of C3-AgNPs aggregated with Hg(II).

of SPR band at 390 nm (Fig. 3). This indicates the Hg(II) ions detection with naked eye, which might be due to induced destabilization and aggregation of C3-AgNPs by Hg(II) (Bothra et al., 2013, 2014; Faghiri & Ghorbani, 2019; Ismail et al., 2019). The selective detection of Hg(II) is attributed to the electrochemical differences of heavy metal ions and $Ag^0$. As Hg(II) has high reduction potential as compared to $Ag^0$, thus, acts as oxidizing agent and could be detected via

colorimetric sensing using UV–visible spectrophotometer (Ismail et al., 2019). The other metal cations; Ag(I), Co(I), Cu(I), Na(I), K(I), Rb(I), Ba(II), Cd(II), Fe(II), Sb(II), Sb (III), Fe(III) to C3-AgNPs solution did not cause any significant color and SPR spectral changes. Hence, these metals have low reduction potentials than $Ag^0$, therefore, they could not act as oxidizing agent, and ultimately, their colorimetric detection using AgNPs is not possible (Bothra et al., 2013, 2014; Faghiri & Ghorbani, 2019; Ismail et al., 2019).

### *3.3. Characterization of C3-AgNPs by FTIR spectroscopy and AFM techniques*

The FT-IR spectrum of C3 (Fig. 4) displayed clear bands at 2922 $cm^{-1}$ (–O-H), 2882 $cm^{-1}$ (=C-H), 2350 $cm^{-1}$ (-C = N), 1627 $cm^{-1}$ (–CO), and 1435 $cm^{-1}$ (C = C) stretching regions. However, in C3-AgNPs formation, the bands exhibited for –OH and –NH groups disappeared completely (Fig. 4), indicating the involvement of hydroxyl group C3-AgNPs stabilization. AFM image (Fig. 5a), indicates the polydispersed and spherical size of the synthesized C3-AgNPs with an average size of 29.93 nm and the range was 5.44–54.4 nm as shown in the size distribution curve (Fig. 5b). From the AFM image recorded after sensing analysis (Fig. 5c), it was found that Hg(II) aggregated the C3-AgNPs, which resulted in huge complexes formation. The AFM results matched the UV–vis analysis, which strengthened the C3-AgNPs application in Hg(II) sensing.

### *3.4. Effect of temperature and salt concentration (NaCl) on stability of C3-AgNPs*

Thermal stability of the synthesized C3-AgNPs (50 μM) was determined at ambient, 60 °C, 70 °C , 80 °C, and 100 °C for 30 min. The UV results of temperature effect (Fig. 6a) have shown prominent decrease and broadening effect of C3-AgNPs absorption band. Chloride ion, a major element of aqueous environment is considered to enhance dissolution as well as aggregation of AgNPs. Therefore, the current investigation also focused on the determination of chloride ion effect on C3-AgNPs. Chloride ions added to the AgNPs solution, affect the rate of aggregation by increasing ionic strength, reducing the electrical double layer around the particles, which ultimately lowers the barrier to aggregation. Furthermore, the chloride ions elevate dissolution of the nanoparticles via increased oxidation of the surface atoms to form silver chloride (AgCl) (Peterson et al., 2016). In the current study, the effect of salt (NaCl) concentration on C3-AgNPs was observed. Various concentrations (10 to 500 μM) of NaCl were treated with C3-AgNPs for 24 h. From the results (Fig. 6b), reduction in C3-AgNPs absorption and stability was seen with increasing NaCl concentration. The observed successive changes in the UV–visible spectra shapes indicated development of silver halide layer and decrease in the adsorption sites for ligand C3 (Espinoza et al., 2012).

### *3.5. Effect of pH on C3-AgNPs stability and its response on Hg (II) sensing*

Since the pH of media has an important role in colloids agglomeration, it is crucial to determine its effect and control on sensitivity and stability of MNPs. In this study, the effect of pH on the stability of C3-AgNPs without and in the presence of Hg(II) was determined. The original pH of C3-AgNPs was in acidic range (4–5). The media pH (2–12) was varied with buffers. From the results, it was seen that there is no change in the absorption spectra (Fig. 7a) recorded at pH 3 to pH 7, whereas increasing the pH (> 8), reduction in absorption band occurred. In addition, at pH 10, a new small peak (600 nm) appeared. Proceeding with further increase in pH to 12, the C3-AgNPs aggregated, and no more changes were observed in the absorption band. Hence, it can be concluded that C3-AgNPs at basic conditions, aggregate, which causes the disturbance in absorption band. Additionally, analyzing the effect of pH on the stability of C3-AgNPs in Hg(II) presence (Fig. 7b) represented no change in the absorbance and intensity of SPR band of C3-AgNPs. Hence, the current sensing Hg(II) protocol could be used at any pH, representing the robustness of this method.

### *3.6. Analytical performance of Hg(II) sensing with C3-AgNPs*

In determining the analytical performance of Hg(II) sensing with C3-AgNPs, the UV–vis spectral profile and the calibration curve (Fig. 8a and b) indicates that the absorbance of SPR band strictly follows a good exponential response to Hg (II) concentrations (0.1–50 μM) with regression constant ($R^2$) of 0.9916. The LOD and LOQ values were found 4.3 μM and 11.0 μM, respectively. These quality parameters represent the practical utility of this method.

### *3.7. Specificity of Hg(II) sensor with competing metals*

A practical metal sensing protocol must be able to achieve high selectivity and response to detect the target metal ions among other potentially interfering ions. The Hg(II) specificity of C3-AgNPs was assessed by competitive experiment in which C3-AgNPs, and 1 equivalent (1 μM) Hg(II) with 1 equivalent (1 μM) of Ag(I), Co(I), Cu(I), Na(I), Rb(I), Ba(II), Cd(II), Fe(II), Sb(II), Fe(III) were treated. The change in absorbance of SBR band corresponding to C3-AgNPs was measured using UV–Vis spectrophotometer. The results (Fig. 9) exhibited that there was no interference from other metal ions in the response of C3-AgNPs detection of Hg(II). Hence, C3-AgNPs specifically recognizes Hg(II) without interfering other metals, and under competitive environment, C3-AgNPs can serve as a selective probe for Hg(II) ions recognition in aqueous medium.

### *3.8. Detection of Hg(II) by C3-AgNPs in real samples of tap water*

The practical application of the synthesized C3-AgNPs was determined for Hg(II) ions recognition in tap water samples taken from Peshawar city. The samples were spiked with 0.1 mM solution of Hg(II) ions and were used after standard pretreatment protocol. The results (Fig. 10) indicated that an SPR band of C3-AgNPs is significantly decreased in the sample of tap water, which concluded the practical utility of this sensing probe, and the designed system can be effectively used to detect Hg(II) in water.

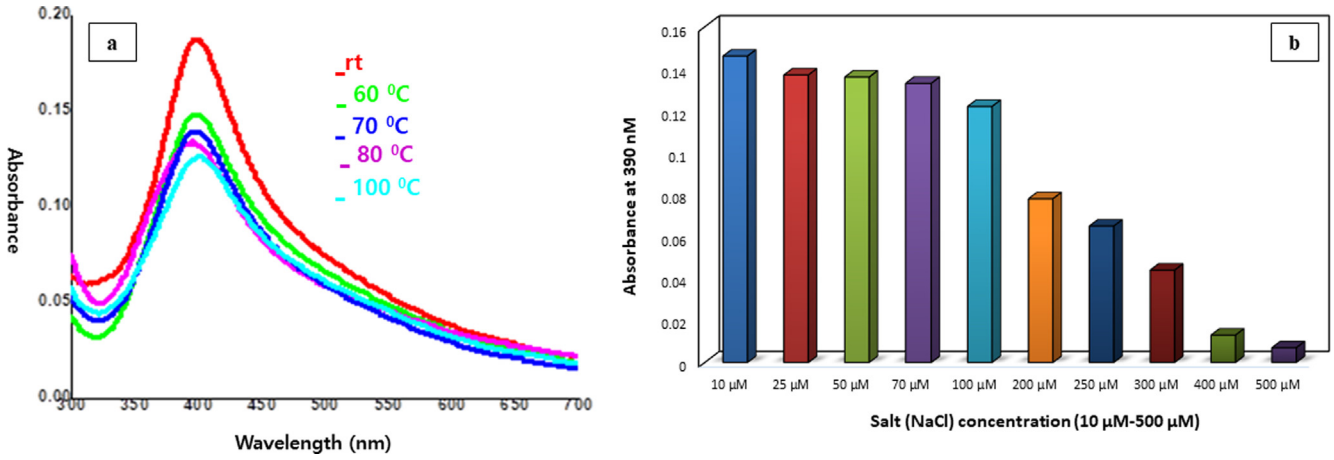


**Fig. 6** UV–Vis spectra showing the effect of (a) temperature and (b) various concentrations of NaCl on stability of C3-AgNPs.

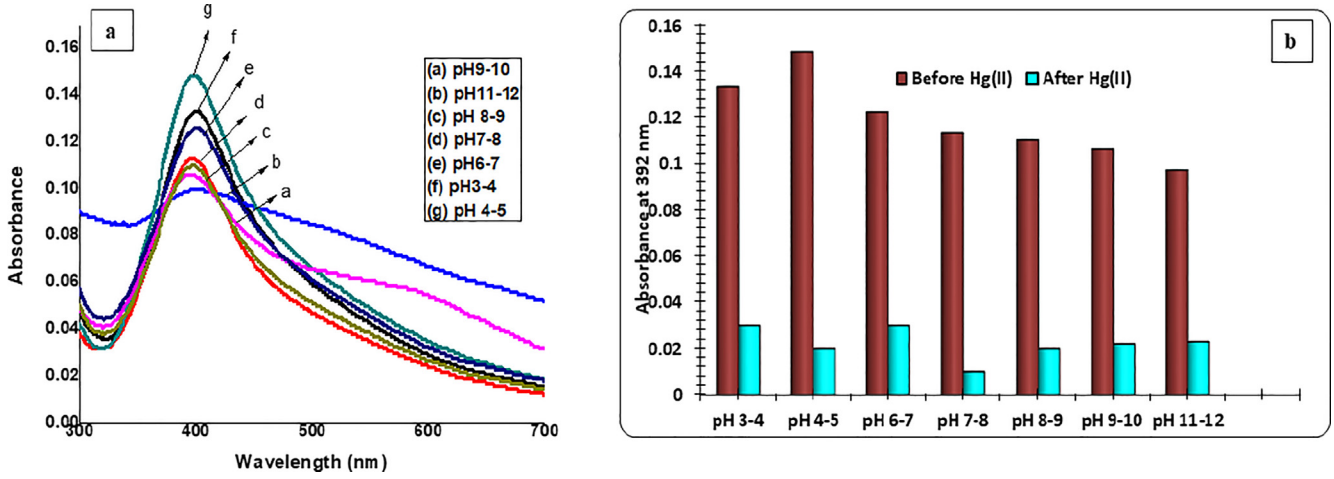


**Fig. 7** UV–Vis spectra showing the (a) effect of pH variability on stability of C3-AgNPs, and (b) bar graph of the effect before and after the addition of Hg(II) ion to C3-AgNPs.

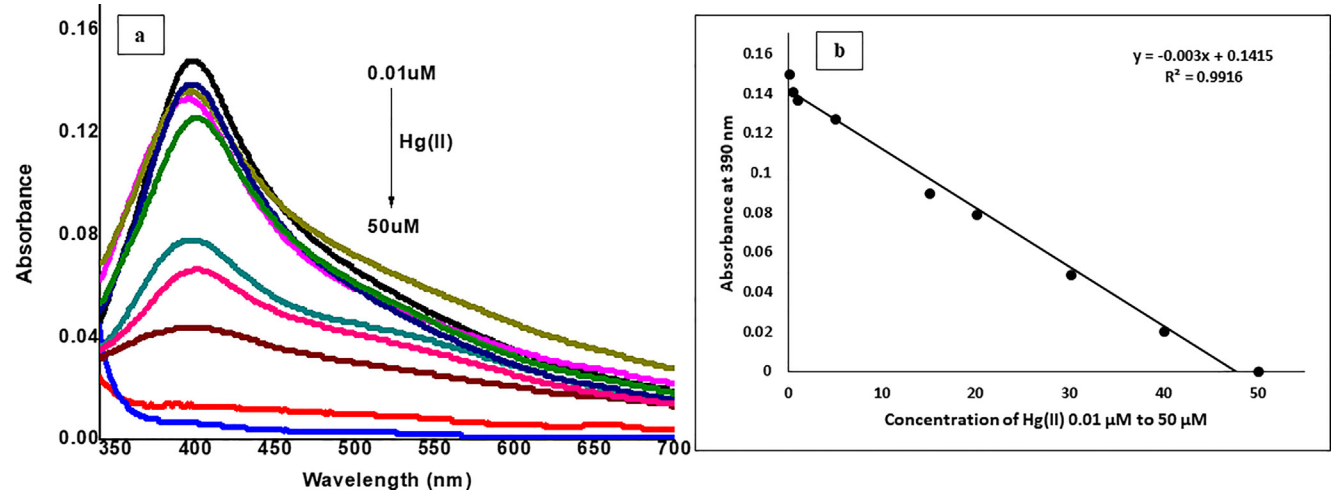


**Fig. 8** (a) UV–Vis spectra, and (b) regression plot of C3-AgNPs in response to various concentrations of Hg(II).

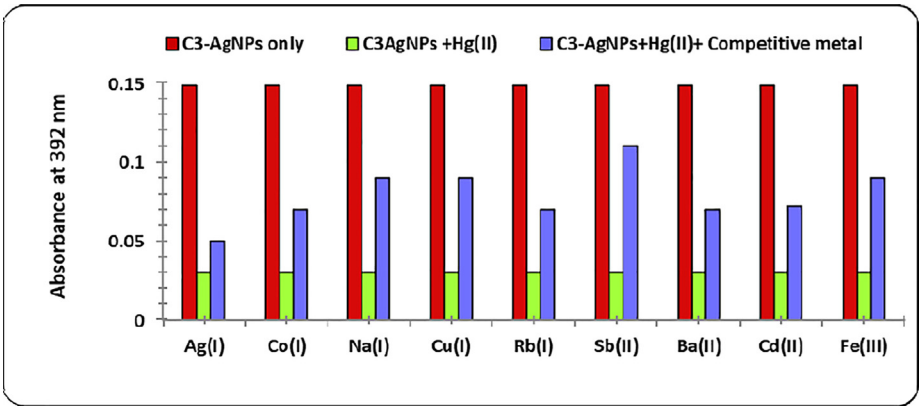


**Fig. 9** Bar graph showing the effect of various metal ions on the absorbance of C3-AgNPs in the presence of Hg(II).

### *3.9. Catalytic application of C3-AgNPs in dyes degradation*

Dyes are conventionally reduced via $NaBH_4$ to non-toxic species, but this degradation proceeds with slow rate. MNPs, due to high surface area have high reducing efficiency, and thus, make the method kinetically viable by lowering the activation energy. For a catalyst to be efficient, the redox potential of AgNPs should be known between the redox potential of donor ($NaBH_4$) and the acceptor (MB, CR) system (Pandey et al., 2020). $NaBH_4$ being a strong nucleophile supply electrons to the degradation reaction, and reduction potential of dye molecules increase due to their adsorption on NPs. AgNPs support in the electron transfer from reducing agent $NaBH_4$ (donor) to dye molecules (acceptor). This uptake of electrons causes degradation of dye molecules by an oxidation–reduction reaction (Pandey et al., 2020). In this work, MB and CR were reduced with $NaBH_4$ and C3-AgNPs. From the results (Fig. 11), it was observed that dyes to which $NaBH_4$ was added (without C3-AgNPs) show very small decrease in the absorption maxima of dyes, indicating slow reduction with $NaBH_4$. However, in the presence of C3-AgNPs, the significant absorption maxima disappeared within 5–10 min. For example, the UV–visible band of MB, which was significantly appeared at 665 nm disappeared in the presence of C3-AgNPs. This indicates the faster reduction of MB. Thus, the study revealed an excellent performance of C3-AgNPs as catalyst.

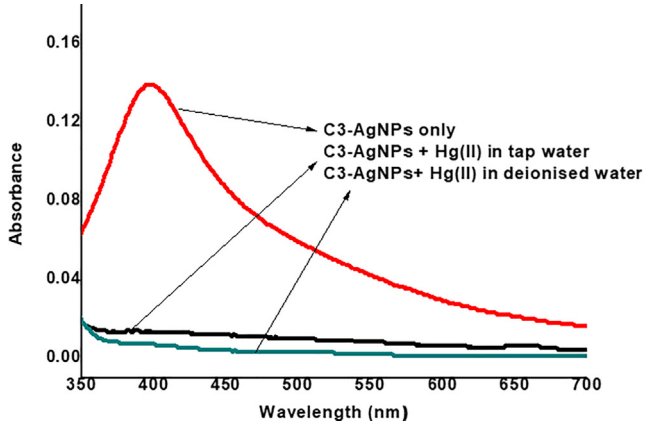


**Fig. 10** UV–Vis spectra of C3-AgNPs detection system of Hg(II) in tap water samples collected from Peshawar.

### *3.10. Anticancer and antibacterial activities of C3-AgNPs*

Besides different treatment strategies for prostate cancer, nanomaterials have attracted the attention of researchers as a novel approach for its treatment. Previous investigations have shown the potent anticancer activity of biogenic AgNPs against various cancers including the prostate (Barabadi et al., 2019; Wang et al., 2020). The ability of C3-AgNPs to induce DU-145 cell death was examined for the first time. The synthesized C3-AgNPs (100 μg/mL) induced DU-145 cells toxicity and caused 94% cell death when treated up to 72 h (Fig. 12). Furthermore, the normal cells (L-929) death was lower (up to 1.5%) as compared to cancer cells, which is the indicative of a selective action of C3-AgNPs. In antibacterial activity (Table 1), C3-AgNPs have shown reasonable inhibition ranging from 7.0 to 18.0 mm and MIC values of 62.5 to 1000 μg/mL for the tested strains. The results of antibacterial effect of the subject C3-AgNPs were consistent to that exhibited by previously synthesized Schiff base AgNPs having inhibition zones of 7–15 mm (Wang et al., 2020), and *Cucumis melo* mediated AgNPs displaying inhibition zones of 7–11 mm (Abdel-Monem et al., 2020).

## 4. Conclusions

A method for the synthesis of 2,2′–((1E,1′E)–(propane–1,3–diylbis(azanylylidene))bis(methanylyl-idene))diphenol (C3) (Schiff base) mediated AgNPs was developed. The whole process for the synthesis of this nanoprobe is efficient, facile, and does not require any complicated and sophisticated instruments. Furthermore, the novel C3-AgNPs were applied for sensing of Hg(II). The designed method could be applied at any pH ranging from 2 to 12, and concentrations from 0.01 μM to 50 μM. Using C3-AgNPs, Hg(II) was precisely detected in the presence of several other competing metallic ions, and in drinking tap water. This study introduces a simple analytical technique for selective heavy metal ions sensing present in drinking water. C3-AgNPs also posed as potential catalyst in MB and CR reduction. In addition, C3-AgNPs induced 94% DU-145 cells death, and have shown significant

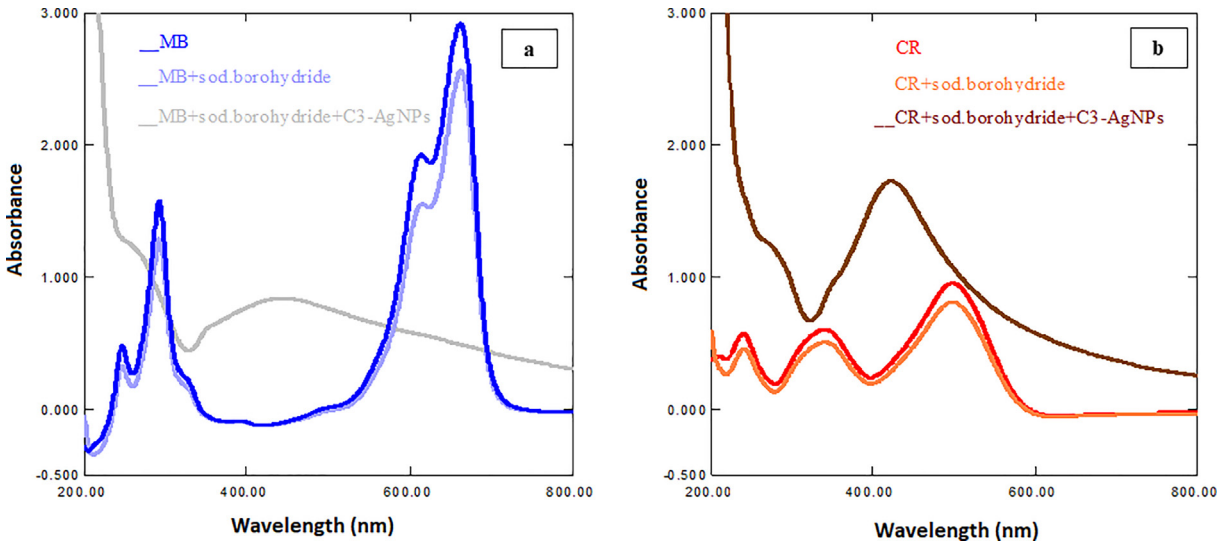


**Fig. 11** UV–Vis spectra of effect of C3-AgNPs on degradation of (a) MB and (b) CR dyes.

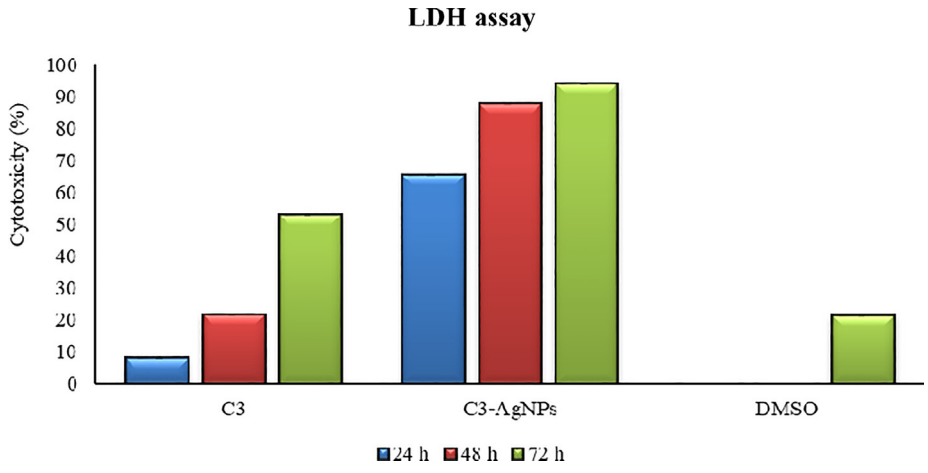


**Fig. 12** Percent (%) anticancer activity (LDH assay) of C3-AgNPs tested on DU-145 cells.

**Table 1** Antibacterial activity by disc diffusion (zone of inhibition, mm) and minimum inhibitory concentration (MIC, μg/mL) methods of synthesized C3 and C3-AgNPs.

| Samples | Disk diffusion (mm) | | | | Minimum inhibitory concentration method (μg/mL) | | | |
|---|---|---|---|---|---|---|---|---|
| | *S. arureus* | *B. subtilis* | *P. aeruginosa* | *E. coli* | *S. aureus* | *B. subtilis* | *P. aeruginosa* | *E. coli* |
| C3 | $8.0 \pm 0.48^{a}$ | $9.0 \pm 0.35^{a}$ | $7.0 \pm 0.39^{a}$ | $7.0 \pm 0.41^{a}$ | $500^{c}$ | $500^{c}$ | $1000^{b}$ | $1000^{c}$ |
| C3-AgNPs | $18.0 \pm 0.27^{b}$ | $18.0 \pm 0.59^{b}$ | $10.0 \pm 0.21^{b}$ | $10.0 \pm 0.26^{b}$ | $250^{b}$ | $250^{b}$ | $500^{a}$ | $500^{b}$ |
| Vancomycin† | $18.0 \pm 0.38^{b}$ | $25.0 \pm 0.26^{c}$ | $12.0 \pm 0.51^{c}$ | $13.0 \pm 0.33^{c}$ | $62.5^{a}$ | 62.5 | $500^{a}$ | $250^{a}$ |
| Streptomycin† | $18.0 \pm 0.19^{b}$ | $24.0 \pm 0.60^{c}$ | $16.0 \pm 0.43^{d}$ | $18.0 \pm 0.57^{d}$ | $62.5^{a}$ | $62.5^{a}$ | $500^{a}$ | $500^{b}$ |

†Represents reference drugs.

Superscript letters (a-f) within the columns represent significant differences ($p < 0.05$) by Tukey's HSD test in the antibacterial activity by disc diffusion (zone of inhibition, mm) and minimum inhibitory concentration (MIC, μg/mL) values of synthesized C3, C3AgNPs, and the reference drugs.

antibacterial potential against all the tested strains. Hence, the synthesized C3-AgNPs could have effective pharmacological and environmental application.

## Declaration of Competing Interest

The authors declare that they have no known competing financial interests or personal relationships that could have appeared to influence the work reported in this paper.

## Acknowledgement

The authors are grateful to Higher Education Commission of Pakistan for their financial support to Aaliya Minhaz and also HEJ (ICCBS-University of Karachi) for providing sample analysis facility. The study was also partially supported by a research grant, 8967/KPK/NRPU/R&D/HEC/2017.

## References

Abdel-Monem, R.A., Khalil, A.M., Darwesh, O.M., Hashim, A.I., Rabie, S.T., 2020. Antibacterial properties of carboxymethyl chitosan Schiff-base nanocomposites loaded with silver nanoparticles. J. Macromol. Sci. A 57, 145–155. https://doi.org/10.1080/10601325.2019.1674666.

Ali, F., Khan, S.B., Kamal, T., Anwar, Y., Alamry, K.A., Asiri, A.M., 2017. Anti-bacterial chitosan/zinc phthalocyanine fibers supported metallic and bimetallic nanoparticles for the removal of organic pollutants. Carbohyd. Polym. 173, 676–689. https://doi.org/10.1016/j.carbpol.2017.05.074.

Anwar, A., Minhaz, A., Khan, N.A., Kalantari, K., Afifi, A.B.M., Shah, M.R., 2018. Synthesis of gold nanoparticles stabilized by a pyrazinium thioacetate ligand: A new colorimetric nanosensor for detection of heavy metal Pd (II). Sens. Actuat. B. Chem. 257, 875–881. https://doi.org/10.1016/j.snb.2017.11.040.

Auría-Soro, C., Nesma, T., Juanes-Velasco, P., Landeira-Viñuela, A., Fidalgo-Gomez, H., Acebes-Fernandez, V., Fuentes, M., 2019. Interactions of nanoparticles and biosystems: microenvironment of nanoparticles and biomolecules in nanomedicine. Nanomaterials 9, 1365. https://doi.org/10.3390/nano9101365.

Balachandramohan, J., Sivasankar, T., 2020. Sonication-assisted synthesis of a new heterostructured schiff base ligand Silver-Guar gum encapsulated nanocomposite as a visible light photocatalyst. J. Microencapsul. 37, 29–40. https://doi.org/10.1080/02652048.2019.1692944.

Barabadi, H., Kamali, K.D., Shoushtari, F.J., Tajani, B., Mahjoub, M.A., Alizadeh, A., Saravanan, M., 2019. Emerging theranostic silver and gold nanomaterials to combat prostate cancer: a systematic review. J. Clust. Sci. 30, 1375–1382.

Bello, B.A., Khan, S.A., Khan, J.A., Syed, F.Q., Mirza, M.B., Shah, L., Khan, S.B., 2017. Anticancer, antibacterial and pollutant degradation potential of silver nanoparticles from *Hyphaene thebaica*. Biochem. Biophys. Res. Commun. 490, 889–894. https://doi.org/10.1016/j.bbrc.2017.06.136.

Bothra, S., Solanki, J.N., Sahoo, S.K., 2013. Functionalized silver nanoparticles as chemosensor for pH, $Hg^{2+}$ and $Fe^{3+}$ in aqueous medium. Sens. Actuat. B. Chem. 188, 937–943. https://doi.org/10.1016/j.snb.2013.07.111.

Bothra, S., Jignasa, N.S., Suban, K.S., John, F.C., 2014. Anion-driven selective colorimetric detection of $Hg^{2+}$ and $Fe^{3+}$ using functionalized silver nanoparticles. RSC. Adv. 4, 1341–1346. https://doi.org/10.1039/C3RA44945A.

Burda, C., Chen, X., Narayanan, R., El-Sayed, M.A., 2005. Chemistry and properties of nanocrystals of different shapes. Chem. Rev. 105, 1025–1102. https://doi.org/10.1021/cr030063a.

Ding, Y., 2019. Organic molecule based chemosensors for biomedical application. Curr. Med. Chem. 26, 3921–3922. https://doi.org/10.2174/0929867326211909191044427.

Dong, G., Duan, K., Zhang, Q., Liu, Z., 2019. A new colorimetric and fluorescent chemosensor based on Schiff base-phenyl-crown ether for selective detection of $Al^{3+}$ and $Fe^{3+}$. Inorg. Chim. Acta. 487, 322–330. https://doi.org/10.1016/j.ica.2018.12.036.

Elahi, N., Kamali, M., Baghersad, M.H., 2018. Recent biomedical applications of gold nanoparticles: A review. Talanta 184, 537–556. https://doi.org/10.1016/j.talanta.2018.02.088.

Espinoza, M.G., Hinks, M.L., Mendoza, A.M., Pullman, D.P., Peterson, K.I., 2012. Kinetics of halide-induced decomposition and aggregation of silver nanoparticles. J. Phy. Chem. C. 116, 8305–8313. https://doi.org/10.1021/jp3011926.

Faghiri, F., Ghorbani, F., 2019. Colorimetric and naked eye detection of trace Hg2+ ions in the environmental water samples based on plasmonic response of sodium alginate impregnated by silver nanoparticles. J. Hazard. Mater. 374, 329–340.

Guo, Q., Shen, X.T., Li, Y.Y., Xu, S.Q., 2017. Carbon nanotubes-based drug delivery to cancer and brain. Curr. Med. Sci. 37, 635–641. https://doi.org/10.1007/s11596-017-1783-z.

Hong, Y.S., Choi, J.Y., Nho, E.Y., Hwang, I.M., Khan, N., Jamila, N., Kim, K.S., 2019. Determination of macro, micro and trace elements in citrus fruits by inductively coupled plasma–optical emission spectrometry (ICP-OES), ICP–mass spectrometry and direct mercury analyzer. J. Sci. Food Agric. 99, 1870–1879. https://doi.org/10.1002/jsfa.9382.

Hwang, I.M., Yang, J.S., Kim, S.H., Jamila, N., Khan, N., Kim, K.S., Seo, H.Y., 2016. Elemental analysis of sea, rock, and bamboo salts by inductively coupled plasma-optical emission and mass spectrometry. Anal. Lett. 49, 2807–2821. https://doi.org/10.1080/00032719.2016.1158831.

Ismail, M., Khan, M.I., Akhtar, K., Seo, J., Khan, M.A., Asiri, A.M., Khan, S.B., 2019. Phytosynthesis of silver nanoparticles; naked eye cellulose filter paper dual mechanism sensor for mercury ions and ammonia in aqueous solution. J. Mater. Sci. Mater. 30, 7367–7383. https://doi.org/10.1007/s10854-019-01049-x.

Jamila, N., Khairuddean, M., Yaacob, S.S., Kamal, N.N.S.N.M., Osman, H., Khan, S.N., Khan, N., 2014. Cytotoxic benzophenone and triterpene from *Garcinia hombroniana*. Bioorg. Chem. 54, 60–67. https://doi.org/10.1016/j.bioorg.2014.04.003.

Jamila, N., Khan, N., Bibi, A., Haider, A., Khan, S.N., Atlas, A., Nishan, U., Minhaz, A., Javed, F., Bibi, A., 2020. *Piper longum* catkin extract mediated synthesis of Ag, Cu, and Ni nanoparticles and their applications as biological and environmental remediation agents. Arab. J. Chem. 13, 6425–6436. https://doi.org/10.1016/j.arabjc.2020.06.001.

Jia, Z., Wei, J., Ren, Y., Zhang, N., Hao, X.Q., Zhu, X., Xu, Y., 2019. A new colorimetric and fluorescent chemosensor based on thiazolyl-hydrazone for sensitive detection of copper ions. J. Iranian Chem. Soc. 1–6. https://doi.org/10.1007/s13738-019-01802-3.

Khan, S.A., Ismail, M., Anwar, Y., Farooq, A., Al-Johny, B.O., Akhtar, K., Shah, Z.A., Nadeem, M., Raza, M.A., Khan, S.B., 2019. A highly efficient and multifunctional biomass supporting Ag, Ni, and Cu nanoparticles through wetness impregnation for environmental remediation. Green Process. Synth. 8, 309–319. https://doi.org/10.1515/gps-2018-0101.

Kumari, R., Saini, A.K., Kumar, A., Saini, R.V., 2020. Apoptosis induction in lung and prostate cancer cells through silver nanoparticles synthesized from *Pinus roxburghii* bioactive fraction. J. Biol. Inorg. Chem. 25, 23–37. https://doi.org/10.1007/s00775-019-01729-3.

Modrzejewska-Sikorska, A., Konował, E., 2020. Silver and gold nanoparticles as chemical probes of the presence of heavy metal ions. J. Mol. Liq. 302,. https://doi.org/10.1016/j.molliq.2020.112559 112559.

Pandey, S., Do, J.Y., Kim, J., Kang, M., 2020. Fast and highly efficient catalytic degradation of dyes using κ-carrageenan stabi-

lized silver nanoparticles nanocatalyst. Carbohydr. Polym. 230,. https://doi.org/10.1016/j.carbpol.2019.115597 115597.

Patil, S.K., Das, D., 2019. A nanomolar detection of mercury (II) ion by a chemodosimetric rhodamine-based sensor in an aqueous medium: Potential applications in real water samples and as paper strips. Spectrochim. Acta A. 210, 44–51. https://doi.org/10.1016/j.saa.2018.11.005.

Peterson, K.I., Lipnick, M.E., Mejia, L.A., Pullman, D.P., 2016. Temperature dependence and mechanism of chloride-induced aggregation of silver nanoparticles. J. Phys. Chem. C. 120, 23268–23275. https://doi.org/10.1021/acs.jpcc.6b07329.

Pungjunun, K., Chaiyo, S., Jantrahong, I., Nantaphol, S., Siangproh, W., Chailapakul, O., 2018. Anodic stripping voltammetric determination of total arsenic using a gold nanoparticle-modified boron-doped diamond electrode on a paper-based device. Microchim. Acta 185, 324. https://doi.org/10.1007/s00604-018-2821-7.

Rao, P.G., Saritha, B., Rao, T.S., 2019. Colorimetric and turn-on fluorescence chemosensor for $Hg^{2+}$ ion detection in aqueous media. J. fluoresc. 29, 353–360. https://doi.org/10.1007/s10895-018-02342-4.

Salarvand, Z., Amirnasr, M., Meghdadi, S., 2019. Colorimetric and fluorescent sensing of Al3+ by a new 2-hydroxynaphthalen based Schiff base‘‘ Off-On” chemosensor. J. Lumin. 207, 78–84. https://doi.org/10.1016/j.jlumin.2018.10.115.

Samerjai, W., Dankhanob, L., Chotimai, P., Jittangprasert, P., Tongraung, P., 2019. Chromogenic Detection of Fe 2+ Using Schiff base-naphthalene-2-ol-modified Silver Nanoparticles. I Iran. J. Sci. Technol. Trans. Sci. 43, 451–456. https://doi.org/10.1007/s40995-017-0425-4.

Singh, J., Dutta, T., Kim, K.H., Rawat, M., Samddar, P., Kumar, P., 2018. Green synthesis of metals and their oxide nanoparticles: applications for environmental remediation. J. Nanobiotechnol. 16, 84. https://doi.org/10.1016/j.matlet.2017.08.078.

Sun, J., Lu, Y., He, L., Pang, J., Yang, F., Liu, Y., 2019. Colorimetric sensor array based on gold nanoparticles: design principles and recent advances. Trends Anal. Chem., 115754 https://doi.org/10.1016/j.trac.2019.115754.

Švehla, J., Žídek, R., Ružovič, T., Svoboda, K., Kratzer, J., 2019. Simple approaches to on-line and off-line speciation analysis of mercury in flue gases with detection by atomic absorption spectrometry: A pilot study. Spectrochim. Acta B. Atom. Spectr. 156, 51–58. https://doi.org/10.1016/j.sab.2019.05.002.

Tan, E., Yin, P., Lang, X., Wang, X., You, T., Guo, L., 2012. Functionalized gold nanoparticles as nanosensor for sensitive and selective detection of silver ions and silver nanoparticles by surface enhanced Raman scattering. Analyst 137, 3925–3928. https://doi.org/10.1039/C2AN35670H.

Wang, Y., Zhang, X., Bai, Y., Li, W., Li, X., Xing, X., et al, 2020. Anticancer and antibacterial activities of silver nanoparticles (AgNPs) synthesized from *Cucumis melo* L. J. Nanosci. Nanotechnol. 20, 4143–4151. https://doi.org/10.1166/jnn.2020.17524.

Ye, Z., Mao, H., Driscoll, C.T., Primary effects of changes in meteorology vs. anthropogenic emissions on mercury wet deposition: A modeling study. Atmos. environ. 198, 215-225. https://doi.org/10.1016/j.atmosenv.2018.10.052.

Zhang, S., Wu, X., Niu, Q., Guo, Z., Li, T., Liu, H., 2017. Colorimetric and highly selective and sensitive colorimetric and fluorescent chemosensor for rapid detection of $Ag^{+}$, $Cu^{2+}$ and $Hg^{2+}$ based on a simple Schiff base. J. fluoresc. 27, 729–737. https://doi.org/10.1002/cjoc.201200852.

Zhao, G., Wang, H., Liu, G., Wang, Z., Cheng, J., 2017. Simultaneous determination of trace Cd (II) and Pb (II) based on Bi/Nafion/reduced graphene oxide-gold nanoparticle nanocomposite film–modified glassy carbon electrode by one–step electrodeposition. Ionics 23, 767–777. https://doi.org/10.1007/s11581-016-1843-6.